Septin 9 interacts with kinesin KIF17 and interferes with the mechanism of NMDA receptor cargo binding and transport

Xiaobo Bai[†], Eva P. Karasmanis[†], and Elias T. Spiliotis*
Department of Biology, Drexel University, Philadelphia, PA 19104

ABSTRACT Intracellular transport involves the regulation of microtubule motor interactions with cargo, but the underlying mechanisms are not well understood. Septins are membrane- and microtubule-binding proteins that assemble into filamentous, scaffold-like structures. Septins are implicated in microtubule-dependent transport, but their roles are unknown. Here we describe a novel interaction between KIF17, a kinesin 2 family motor, and septin 9 (SEPT9). We show that SEPT9 associates directly with the C-terminal tail of KIF17 and interacts preferentially with the extended cargo-binding conformation of KIF17. In developing rat hippocampal neurons, SEPT9 partially colocalizes and comigrates with KIF17. We show that SEPT9 interacts with the KIF17 tail domain that associates with mLin-10/Mint1, a cargo adaptor/scaffold protein, which underlies the mechanism of KIF17 binding to the NMDA receptor subunit 2B (NR2B). Significantly, SEPT9 interferes with binding of the PDZ1 domain of mLin-10/Mint1 to KIF17 and thereby down-regulates NR2B transport into the dendrites of hippocampal neurons. Measurements of KIF17 motility in live neurons show that SEPT9 does not affect the microtubule-dependent motility of KIF17. These results provide the first evidence of an interaction between septins and a nonmitotic kinesin and suggest that SEPT9 modulates the interactions of KIF17 with membrane cargo.

INTRODUCTION

Microtubule (MT) motors of the kinesin family are essential for the long-range intracellular transport of membrane organelles, proteins, and mRNA (Hirokawa et al., 2009). Spatiotemporal control and specificity in kinesin-mediated transport is achieved through regulation of kinesin interactions with cargo and MTs (Verhey and Hammond, 2009). Scaffolding and adaptor proteins mediate the interaction of kinesins with specific cargo and modulate motor activity in coordination with regulatory molecules (Akhmanova and Hammer, 2010; Fu and Holzbaur, 2014). On MTs, kinesin motility is regulated by tubulin isoforms and posttranslational modifications,

as well as by MT-associated proteins, which affect the directionality, velocity, and processivity of transport (Verhey and Gaertig, 2007; Atherton et al., 2013; Sirajuddin et al., 2014).

The kinesin 2 family motor KIF17 is a homodimeric plus end–directed motor that mediates the transport of synaptic receptors, channels, and mRNA in neuronal dendrites (Chu et al., 2006; Kayadjanian et al., 2007; Takano et al., 2007; Yin et al., 2011, 2012). KIF17 is also involved in the nucleocytoplasmic and intraflagellar transport of transcriptional factors and ciliary proteins (Macho et al., 2002; Jenkins et al., 2006; Dishinger et al., 2010). KIF17 consists of an N-terminal motor head domain, a neck and stalk region with coiled-coil domains, and a cargo-binding C-terminal tail (Wong-Riley and Besharse, 2012). In the absence of cargo, the motor domain of KIF17 is autoinhibited by the stalk and C-terminal tail, which interfere with MT binding and processive motility (Hammond et al., 2010; Espenel et al., 2013). In addition, the C-terminal tail of KIF17 inhibits the catalytic activity of the motor domain and interacts directly with MTs (Acharya et al., 2013). Among the known cargo of KIF17, the N-methyl-D-aspartate (NMDA) receptor subunit B (NR2B) associates with KIF17 by a mechanism that involves the mLin scaffolding complex. The C-terminal tail of KIF17 interacts directly with the PDZ1 domain of mLin-10 (Mint1/X11), which in turn binds NR2B

via the mLin-7 subunit of the mLin-10/mLin-2/mLin-7 complex (Jo et al., 1999; Setou et al., 2000).

Septins are a family of G-proteins, which form hetero-oligomeric and polymeric structures that function as scaffolds and diffusion barriers, controlling the localization of membrane and cytoplasmic proteins (Kinoshita, 2006; Caudron and Barral, 2009; Mostowy and Cossart, 2012; Spiliotis and Gladfelter, 2012). Mammalian septins interact with MTs and are involved in Golgi–to–plasma membrane vesicle transport and chromosome alignment (Nagata et al., 2003; Spiliotis et al., 2005, 2008; Sellin et al., 2012; Bai et al., 2013). Septins have been shown to interact with centromere-associated protein E (CENP-E), a mitotic kinesin–like motor that links kinetochores to the ends of spindle MTs (Zhu et al., 2008). However, the role of septins in MT-dependent transport of membrane cargo is unknown.

RESULTS AND DISCUSSION
SEPT9 interacts directly with the C-terminal tail of KIF17 in its cargo-binding conformation

Previous work showed that septins associate with the C-terminal tail of a mitotic kinesin (Zhu et al., 2008). Given the role of the C-terminal tail of KIF17 in cargo binding and regulation of KIF17 motor activity and localization (Setou et al., 2000; Guillaud et al., 2003; Dishinger et al., 2010; Hammond et al., 2010; Acharya et al., 2013; Espenel et al., 2013), we used a glutathione S-transferase (GST)–tagged KIF17 tail (amino acids 850–1029) as bait to probe for potential interactions with septins. In embryonic (embryonic day 18 [E18]) rat brain homogenates (Figure 1A) and Madin–Darby canine kidney (MDCK) cell lysates (Supplemental Figure S1A), we found that GST-KIF17(850-1029) pulls down SEPT9. Consistent with this finding, endogenous KIF17 and SEPT9 coimmunoprecipitated in lysates from whole rat brains and MDCK and HEK293 cells (Figure 1B and Supplemental Figure S1, B and C).

Next we examined the localization of SEPT9 and KIF17 in primary rat embryonic (E18) hippocampal neurons using antibodies whose specificity was tested by treatment with antigenic peptides and staining with secondary antibody only (Supplementary Figure S2, A and C). KIF17 had a punctate and diffuse distribution (Figure 1C). SEPT9 was similarly punctate and diffuse (Figure 1C), but short filaments were also observed (blue arrows in Figure 1C and Supplemental Figure S2B). Wide-field and superresolution structured illumination microscopy (SIM) showed that SEPT9 colocalizes with a fraction of KIF17 puncta (~10% of total KIF17), which are found in dendritic shafts and branch points (Figure 1, C and D) and occasionally at postsynaptic densities; $16 \pm 3\%$ (17 cells) of SEPT9/KIF17-containing puncta colocalized with PSD95.

To test whether SEPT9 associates directly and specifically with KIF17, we performed in vitro binding assays with recombinant septins and KIF17 domains (Figure 2A). The C-terminal tail of KIF17 pulled down recombinant septin 9 (SEPT9) but not SEPT2 (Figure 2B) or SEPT6/7 (Supplemental Figure S3A), which are known to heteromerize with SEPT9 (Kim et al., 2011; Sellin et al., 2011). In vitro binding assays with the motor head domain KIF17(1-339) and KIF17(1-490), which consists of the head and neck domains (Figure 2A), as well as KIF17(340-849), which contains the neck and stalk domains, showed that SEPT9 interacts preferentially with the C-terminal tail of KIF17 (Figure 2, C and D, and Supplemental Figure S3, B and C). Thus SEPT9 interacts directly with KIF17 via its C-terminal cargo-binding domain.

Because the C-terminal tail of KIF17 exists in an extended cargo-binding or a "closed" autoinhibitory conformation (Hammond et al., 2010), we tested whether SEPT9 binding is affected by the confor-

mation of the KIF17 tail. We performed coimmunoprecipitations with myc-tagged wild-type KIF17 or the mutant KIF17(G754E), which maintains an extended cargo-binding conformation (Hammond et al., 2010). We found that the amount of endogenous SEPT9 that coimmunoprecipitated with KIF17(G754E) was 1.5- to 2.5-fold greater than with wild-type KIF17 (Figure 3A). A similar difference was observed in the amount of SEPT9–green fluorescent protein (GFP) that coimmunoprecipitated with myc-KIF17(G754E) versus myc-KIF17 (Supplemental Figure S3, D and E). In agreement with SEPT9 binding to the extended conformation of KIF17, SEPT9-mCherry comigrated with GFP-KIF17(G754E) in hippocampal neurons (Figure 3B and Supplemental Movie S1). Taken together, these data indicate that SEPT9 interacts directly and preferentially with the C-terminal tail of KIF17 in its cargo-binding conformation, raising the possibility that SEPT9 is involved in the interactions of KIF17 with membrane cargo.

SEPT9 competes with mLin-10/Mint1 for binding to the tail of KIF17

KIF17 was first discovered as a kinesin motor that mediates the transport of NR2B cargo (Setou et al., 2000). Mechanistically, KIF17 associates with NR2B-carrying vesicles through the mLin-2/mLin-7/mLin-10 complex (Jo et al., 1999; Setou et al., 2000). Whereas mLin-7 binds the cytoplasmic tail of NR2B, mLin-10 interacts with the C-terminal half of the KIF17 tail through its PDZ1 domain (Jo et al., 1999; Setou et al., 2000). Given that SEPT9 associates with the tail of KIF17 and is highly expressed in rodent brains during mid to late gestation (E15–E18), which marks the onset of NR2B, KIF17, and mLin2/7/10 expression (Setou et al., 2000; Tsang et al., 2011), we sought to examine whether SEPT9 affects the mechanism of interaction between KIF17 and NR2B.

To determine the binding site of SEPT9 with respect to mLin-10, we performed in vitro binding assays with the C-terminal tail fragments KIF17(850-980) and KIF17(981-1029). We found that SEPT9 interacts preferentially with KIF17(981-1029) (Figure 4A), which contains the binding site of mLin-10. Because the KIF17-mLin-10 interaction involves the last three amino acids (EPL) of the C-terminal tail of KIF17 (Setou et al., 2000), we tested whether the EPL sequence is also required for SEPT9-KIF17 binding. Mutating the EPL sequence into AAA resulted in twofold-to-threefold reduction in the binding of full-length SEPT9 to KIF17(981-1029) (Figure 4B). Thus SEPT9 and the PDZ1 domain of mLin-10 interact with the C-terminal tail of KIF17 through overlapping binding sites and may compete for KIF17. Indeed, binding of the PDZ1-containing mLin-10(653-839) to KIF17(981-1029) was reduced by 50% in the presence of SEPT9 (Figure 4, C and D). In N2a cells, coimmunoprecipitation of endogenous KIF17 with GFP-mLin-10 was also reduced in the presence of SEPT9 (Figure 4, E and F).

To test whether SEPT9 has a similar effect on the interaction of KIF17 with mLin-10 in hippocampal neurons, we overexpressed SEPT9-GFP in hippocampal neurons and analyzed the localization of endogenous KIF17 with respect to mLin-10. Expression of SEPT9-GFP decreased the punctate distribution of KIF17 in dendritic processes (Figure 4, H and I) and reduced the percentage of KIF17-positive mLin-10 puncta from 37.6 ± 2.7 to $18.7 \pm 1.8\%$ per 10 μm of dendritic process (Figure 4G). Superresolution SIM imaging of endogenous KIF17, SEPT9, and mLin-10 showed that only $9 \pm 3\%$ (17 cells) of KIF17/SEPT9 puncta contained mLin-10 (Figure 4J), and SEPT9 was similarly absent from KIF17/mLin-10 puncta (Figure 4K). Taken together with the biochemical evidence of a physical interference, these data indicate that SEPT9 competes with mLin-10 for binding to KIF17.
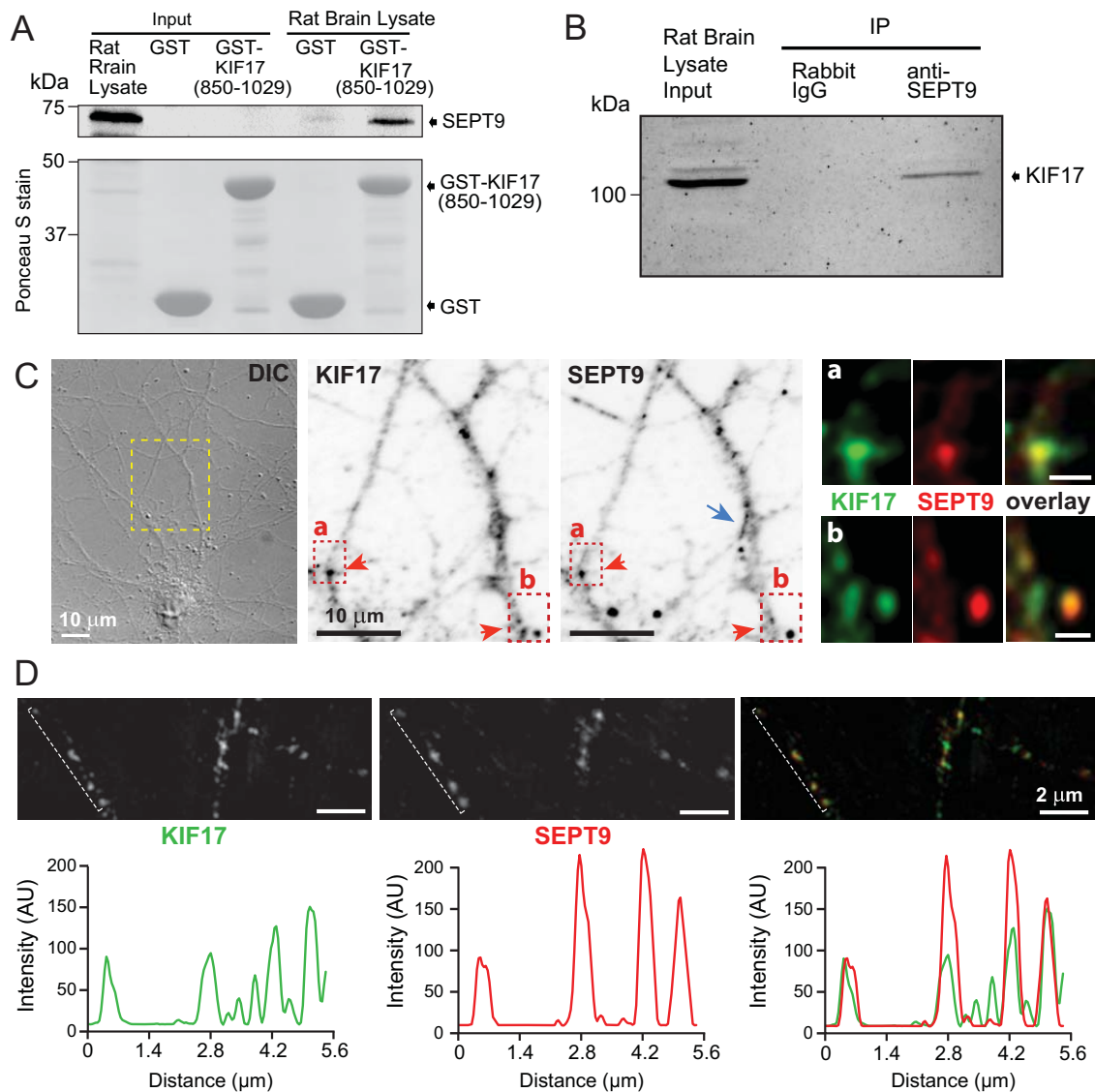
FIGURE 1: SEPT9 interacts and partially colocalizes with KIF17. (A) Western blot (top) of GST pull downs from embryonic (E18) rat brain homogenate. Ponceau S–stained membrane (bottom) shows the presence of GST proteins. Input is 2% of total lysate. (B) Western blot of immunoprecipitates from rat brain homogenates. Input is 2% of total lysate. (C) Differential interference contrast (DIC) and fluorescence microscopy images of a rat hippocampal neuron (days in vitro [DIV] 14) stained for KIF17 and SEPT9. Red arrows point to colocalizing SEPT9 and KIF17 puncta. (a, b) Regions outlined by dotted lines shown in higher magnification (scale bars, ~2 μm). Blue arrow points to filamentous SEPT9. (D) Superresolution SIM imaging of KIF17 and SEPT9 puncta in hippocampal neurons. Line scans show the fluorescence intensity profiles of KIF17 and SEPT9 along the outlined region.

SEPT9 down-regulates the transport of NR2B cargo without interfering with the motility of KIF17

Given that SEPT9 interferes with the binding of mLin-10 to KIF17, we asked whether SEPT9 affects the intracellular transport of NR2B. We tested how SEPT9 affects, first, the localization of endogenous NR2B and, second, the transport of newly synthesized GFP-NR2B. Hippocampal neurons were transfected with SEPT9-GFP or GFP, and cells were stained for endogenous NR2B using a gentle permeabilization protocol that preserved the localization of NR2B in both surface and intracellular membranes. In contrast to control cells, in which NR2B outlined each dendrite, NR2B was weakly present in the dendrites of SEPT9-GFP–expressing cells (Figure 5, A and B, insets), and the mean intensity of NR2B was reduced by 42%

(Figure 5C). This effect was specific to NR2B, as SEPT9-GFP overexpression did not affect the surface levels of the potassium channel Kv4.2 (Figure 5D), which is also transported by KIF17 (Chu *et al.*, 2006). Although it is unknown whether the C-terminal EPL motif of KIF17 interacts with Kv4.2, our results suggest that SEPT9 does not interfere with the mechanism of KIF17-Kv4.2 binding, which may be different from how KIF17 binds NR2B.

Next we transfected hippocampal neurons with GFP-NR2B and SEPT9-mCherry or mCherry and analyzed the distribution of surface and total GFP-NR2B. Staining of live neurons with an anti-GFP antibody before fixation showed that GFP-NR2B is properly transported and incorporated into the surface membranes of dendrites, forming an array of clusters that outline each dendrite (Figure 5E).
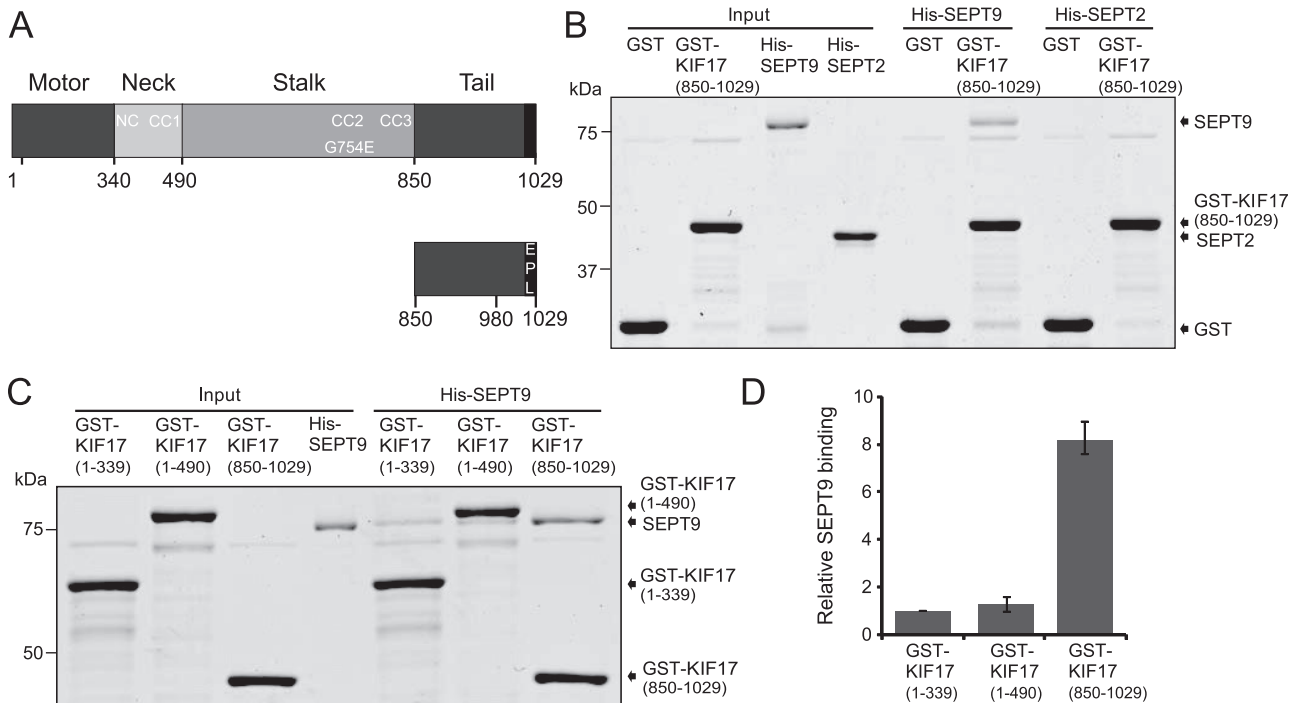
FIGURE 2: SEPT9 associates directly with the C-terminal tail of KIF17. (A) Schematic shows the boundaries of the motor, neck, stalk, and tail domains of KIF17. Positions of the G754E mutation, neck coil (NC), and coiled coil (CC) domains and the EPL site involved in the binding of the PDZ1 domain of mLin-10/Mint1. (B) Coomassie-stained SDS–PAGE gel shows the cosedimentation of His-SEPT9 or His-SEPT2 with GST or GST-KIF17(850-1029). (C) Coomassie-stained gel shows the cosedimentation of His-SEPT9 with GST-tagged KIF17(1-339), KIF17(1-490), or KIF17(850-1029). (D) Bar graph shows relative His-SEPT9 binding after quantification of His-SEPT9 band intensities and normalization to GST-tagged protein bands. The amount of His-SEPT9 cosedimented with GST-KIF17(1-339) was set to 1. Error bars correspond to the highest and lowest values from three independent experiments.

Compared to control cells, surface levels of GFP-NR2B decreased by 30% (Figure 5F). This reduction in surface NR2B was not due to a local defect in membrane targeting within individual dendrites, because total GFP-NR2B fluorescence was reduced in all dendrites (Figure 5G), and GFP-NR2B clusters decreased by 40% from 5.6 ± 0.4 to 3.3 ± 0.3 ($p < 0.0001$) per 10 µm of dendrite. Moreover, this quantitative effect was not due to variations in GFP-NR2B expression, which was similar between cell populations that expressed mCherry and SEPT9-mCherry (66 ± 8 vs. 71 ± 8 arbitrary units/µm², $p = 0.6$). Thus SEPT9 appears to down-regulate the long-range transport of NR2B.

Taken together with the diminished binding of mLin-10 to KIF17, our results suggest that SEPT9 affects the mechanism of KIF17-mediated transport of NR2B at the level of cargo–motor binding. Down-regulation of NR2B transport, however, could also stem from alterations in the motility KIF17. To address this possibility, we used total internal reflection fluorescence microscopy (TIRF) microscopy to image the motility of GFP-KIF17 in rat hippocampal neurons that expressed SEPT9-mCherry or mCherry. Quantification of GFP-KIF17 motility showed that SEPT9 overexpression had no statistically significant effect on the velocity and run lengths of KIF17 (Figure 5H). Moreover, SEPT9 overexpression did not affect the percentage of KIF17 puncta that were mobile (Figure 5I). Therefore the activity and motile properties of KIF17 are not altered by SEPT9.

Our results provide the first evidence of septin involvement in kinesin–cargo interactions and raise the possibility that septins may act as regulators of cargo–motor binding. Similar to other scaffolding proteins (e.g., Hook-1) that bind kinesins (Walenta

et al., 2001; Bielska et al., 2014), septins interact with both MTs and cell membranes (Spiliotis and Gladfelter, 2012). Of interest, SEPT9 has been reported to associate with the c-Jun-N-terminal kinase (JNK), which is reminiscent of the JNK-interacting proteins (JIPs) that interact with kinesin 1 and the dynein/dynactin complex (Verhey et al., 2001; Gonzalez et al., 2009; Sun et al., 2011; Fu and Holzbaur, 2013). In contrast to JIP1, which regulates motor activity by relieving the autoinhibition of kinesin 1 (Blasius et al., 2007; Fu and Holzbaur, 2013), SEPT9 is not likely to affect the autoinhibition of KIF17, because, first, SEPT9 interacts preferentially with the C-terminal tail of KIF17 in its extended cargo-binding conformation and, second, SEPT9 does not affect the motility of KIF17 in living neurons.

Our results suggest that SEPT9 could affect the loading of cargo to KIF17 or trigger the release of cargo from KIF17. It is unknown whether SEPT9 associates with specific organelles or membrane cargo, but SEPT2 and SEPT7 have been reported to interact respectively with the cytoplasmic tail of the GLAST glutamate receptor and the adaptor protein AP3 (Kinoshita et al., 2004; Baust et al., 2008). Thus SEPT9 could link KIF17 to specific cargo directly or indirectly through hetero-oligomerization with other membrane-bound septin subunits. Alternatively, septins could influence cargo selection by rendering the tail of KIF17 unavailable to other cargo adaptor/scaffold proteins (e.g., mLin-10). In the context of brain development, high levels of SEPT9 expression may inhibit the transport of NR2B in late gestation when KIF17, NR2B, and the mLin10 complex are initially expressed (Setou et al., 2000; Tsang et al., 2011).
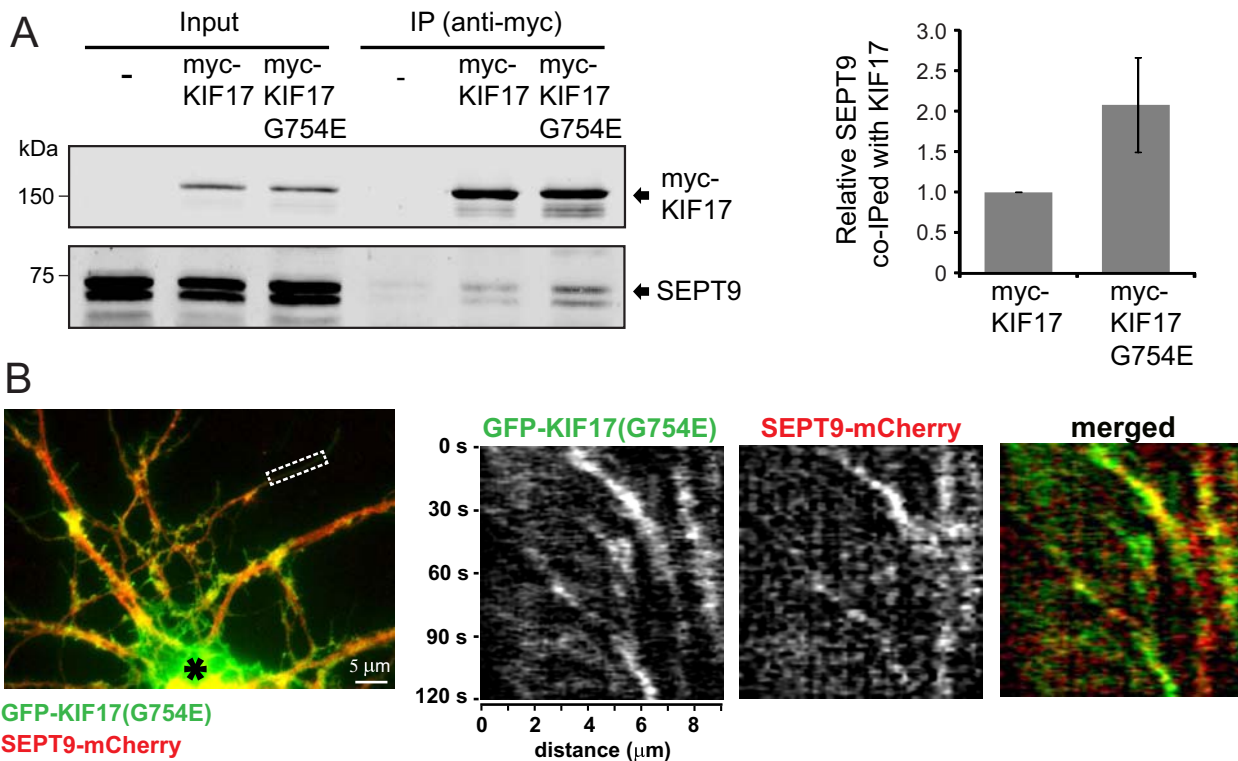
FIGURE 3: SEPT9 interacts preferentially and comigrates with the extended cargo-binding conformation of KIF17(G754E). (A) Western blots of coimmunoprecipitations of endogenous SEPT9 with myc-tagged KIF17 or KIF17(G754E) from HEK293 lysates. Input is 2% of total lysate. Bar graph shows the relative difference in the amount of SEPT9 that coimmunoprecipitated with myc-KIF17 vs. myc-KIF17(G754E). After background subtraction, protein band intensities were quantified and the ratio of SEPT9 to KIF17 was calculated; the ratio of SEPT9 to myc-KIF17 was set to 1. Error bars show the minimum and maximum values from three independent experiments. (B) Rat hippocampal neurons were transfected with GFP-KIF17(G754E) (green) and SEPT9-mCherry (red) and imaged by TIRF microscopy. Image shows the dendritic processes of a hippocampal neuron; cell body is denoted with an asterisk. Kymographs show the comigration of GFP-KIF17(G754E) and SEPT9-mCherry in the region outlined with a dotted rectangle (Supplemental Movie S1).

The inhibition of KIF17-mLin10 binding by SEPT9, which interacts preferentially with the cargo-binding conformation of KIF17, and the partial colocalization of SEPT9 with KIF17 suggest that SEPT9 triggers the release of cargo by binding KIF17 selectively and/or transiently. Thus SEPT9 may provide a new mechanism for the unloading of KIF17 cargo under the control of spatial and temporal cues. Given that septins localize to dendritic branch points and at the base of protrusive structures, including dendritic spines, axonal filopodia, and primary cilia (Tada *et al.*, 2007; Xie *et al.*, 2007; Hu *et al.*, 2010, 2012), septins could mediate the release of cargo at these intracellular sites and compartments. Future studies will further explore a septin-mediated regulation of cargo–motor interactions and its significance for the spatiotemporal control of intracellular transport.

MATERIALS AND METHODS
Cells and transfections
MDCKII/G, N2a, and HEK293 cells were grown in DMEM with 10% fetal bovine serum and transfected with Lipofectamine 2000 (Invitrogen, Grand Island, NY; Dolat *et al.*, 2014). Primary rat embryonic (E18) hippocampal neurons were obtained from the MINS Neuron Culture Service Center (University of Pennsylvania, Philadelphia, PA), cultured in Neurobasal medium supplemented with B27 (GIBCO, Grand Island, NY) and cytosine *d*-D-arabinofuranoside, and transfected with Lipofectamine LTX (Invitrogen).

Plasmids
GST-tagged fragments of KIF17 were made by PCR amplification from a plasmid encoding for myc-KIF17 (gift from Geri Kreitzer, Weill Cornell Medical College, New York, NY; Jaulin and Kreitzer, 2010) and cloning into pGEX-KT-ext vector. GFP-KIF17 was made by inserting the full-length KIF17 sequence into pEGFP-C1. His-KIF17(850–1029) was created by inserting the PCR-amplified fragment into pET-28a(+). All mutations and truncations were made with the QuikChange II Site-Directed Mutagenesis Kit (Agilent Technologies, Santa Clara, CA). The plasmids encoding for His-Mint1/mLin-10(653–839) was a gift from Angela Ho (Boston University, Boston, MA; Matos *et al.*, 2012), and GFP-Mint1/mLin-10 was a gift from Angelika Barnekow (University of Münster, Münster, Germany). C-terminal fusions of SEPT9_i1 with GFP or mCherry were made by PCR amplifying each gene and cloning into the *Xho*I and *Hind*III sites of the pEGFP-N1 or pmCherry-N1 plasmids. Plasmids encoding for histidine (His)-tagged SEPT9_i1, SEPT2 and SEPT6-His-SEPT7 were previously described (Bai *et al.*, 2013). Myc-SEPT9 was made by PCR amplifying SEPT9_i1 using the primers 5'-CGTAAGCTTGCATGAAGAAGTCTTACTC-3' and 5'-GTACTCGAGCATCTCTGGGGCTTC-3' and inserting the amplified fragment into pcDNA 3.1/myc-His A. pCI-EGFP-NR2b wt (plasmid 45447; Addgene, Cambridge, MA) was a gift from Andres Barria and Robert Malinow (Cold Spring Harbor Laboratory, Cold Spring Harbor, NY; Barria and Malinow, 2002).
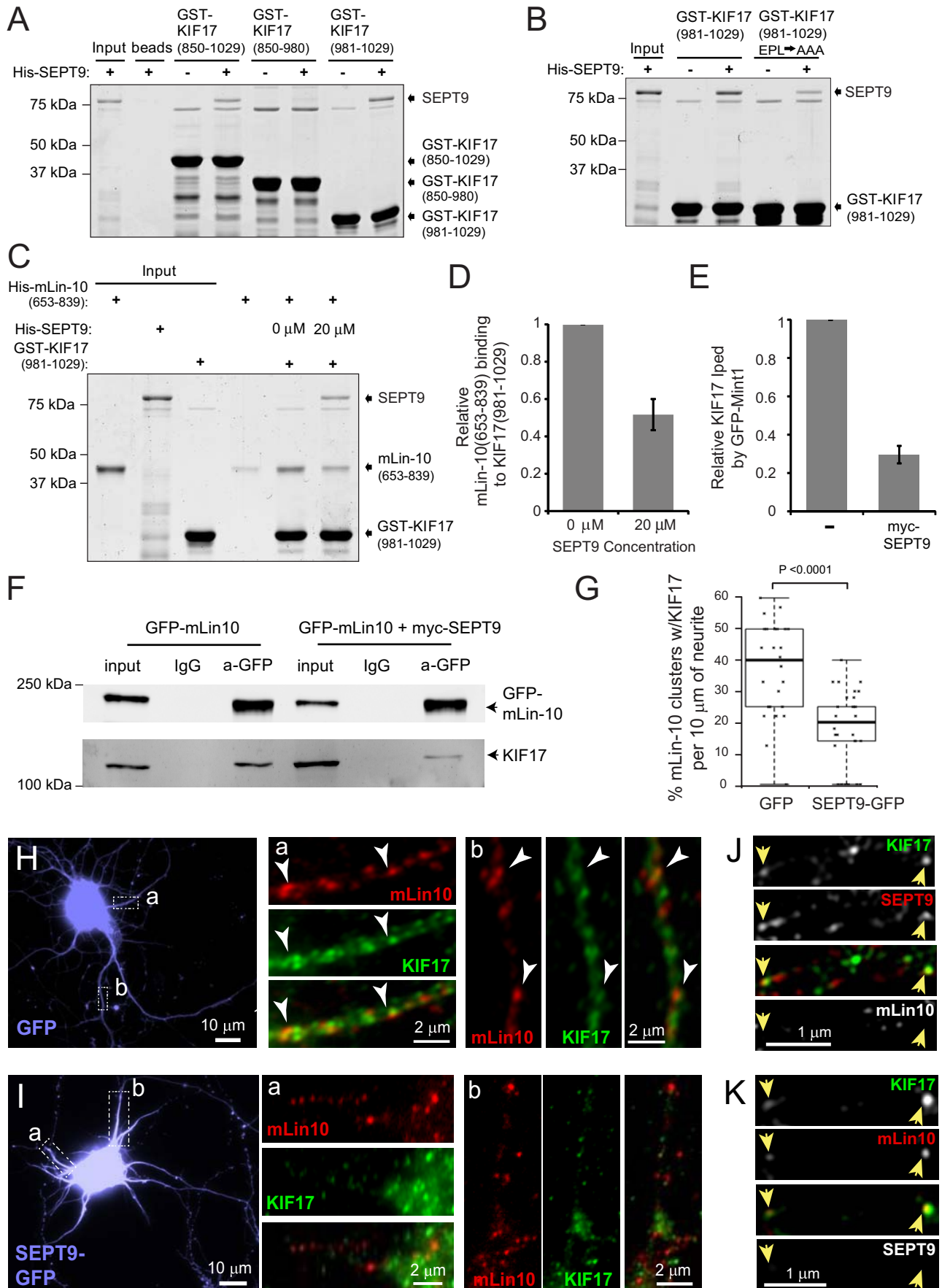
Protein purification and binding assays

Bacterial expression and purification of recombinant proteins were performed as previously (Bai *et al.*, 2013). In protein binding assays, GST-tagged proteins (10 µg) were first coupled to GSH agarose 4B beads (Macherey Nagel, Bethlehem, PA), which were subsequently incubated for 30 min with His-tagged proteins in GST pull-down buffer (50 mM 4-(2-hydroxyethyl)-1-piperazineethanesulfonic acid [HEPES], 150 mM NaCl, 2 mM ethylene glycol tetraacetic acid, 0.1% Triton X-100, 1 mM phenylmethylsulfonyl fluoride, and 5 mM dithiothreitol, pH 7.4). For competitions assays, beads were incubated for 10 min with His-SEPT9 and then mixed and incubated for 30 min with mLin-10(653-839). After washing (5×) with GST pull-down buffer, beads were resuspended in SDS loading buffer, boiled, and loaded onto SDS–PAGE gels, which were stained with Coomassie brilliant blue.

GST pull downs and immunoprecipitations

MDCK cells (3×10^6) and an embryonic (E18) rat brain (BrainBits, Springfield, IL) were homogenized in GST pull-down buffer for 1 h at 4°C. Cell debris was pelleted by centrifugation, and supernatants were incubated for 30 min with GST-KIF17(850-1029)–bound beads. After washing, beads were resuspended in SDS loading buffer, boiled, and loaded onto SDS–PAGE gels, which were transferred to nitrocellulose membranes and blotted with a SEPT9 antibody (Proteintech, Rosemont, IL). Coimmunoprecipitations of KIF17 and SEPT9 were performed by lysing E18 rat brains and MDCK and HEK293 cells for 4 h at 4°C in buffer containing 10 mM HEPES, pH 7.5, 150 mM NaCl, 0.25% Triton X-100, and protease inhibitors (EMD Millipore, Darmstadt, Germany). After spinning at $14,000 \times g$ for 3 min, supernatants were precleared overnight at 4°C with protein A beads (ThermoFisher Scientific, Grand Island, NY) and subsequently, incubated for 12 h at 4°C with 4 µg of rabbit anti-SEPT9 (Proteintech) or preimmune rabbit immunoglobulin G (IgG). Complexes were captured by incubating overnight with 50 µl of protein A beads, which were preblocked in lysis buffer containing 5% bovine serum albumin. Beads were washed (5×) in lysis buffer, boiled in SDS loading buffer, and run on 10% SDS–PAGE. Gels were Western blotted with goat anti-KIF17 (1:500; Santa Cruz Biotechnology, Dallas, TX) and rabbit anti-SEPT9 (1:1000; Proteintech). Coimmunoprecipitation of endogenous SEPT9 with myc-KIF17 was similarly performed after transfection of HEK293 cells with myc-KIF17 constructs. Coimmunoprecipitations of myc-KIF17 and GFP-tagged SEPT9 were performed after transfecting HEK293 cells with plasmids encoding for myc-KIF17 (wild type or G754E) and GFP or SEPT9-GFP. Cells were lysed in buffer containing 25 mM Tris-HCl (pH 7.5), 150 mM NaCl, 1 mM EDTA, 0.5% Triton X-100, and protease inhibitors (EMD Millipore). Lysates were precleared with protein A beads (ThermoFisher) and incubated overnight with rabbit anti-GFP (A6455; Invitrogen) and subsequently with protein A beads for 6 h at 4°C. Beads were washed (5×) with lysis buffer, boiled in SDS loading buffer, and run on 10% SDS–PAGE. Western blots were performed with mouse anti-myc (Roche, Branchburg, NJ) and anti-GFP (A11120; Invitrogen) and secondary antibodies conjugated to infrared dyes. Membranes were scanned and protein bands were quantified with the Odyssey system (LI-COR, Lincoln, NE).

Coimmunoprecipitation of endogenous KIF17 with GFP-mLin-10 (Figure 4F) was performed by transfecting N2a with plasmids encoding for GFP-mLin10 and myc-SEPT9_i1. Cells were lysed in ice-cold RIPA buffer (50 mM Tris, 1% Triton X-100, 0.1% SDS, 150 mM NaCl, pH 8.0) and protease inhibitors (EMD Millipore). Lysates were precleared with protein A beads (ThermoFisher) and incubated with rabbit IgG or anti-GFP (A6455; Invitrogen) and protein A beads overnight at 4°C. Beads were washed with TBST (0.05% Tween-20, Tris-buffered saline, pH 7.4), boiled in SDS loading buffer, and run on 10% SDS–PAGE. Western blots were performed with mouse anti-rat Mint1/mLin-10 (clone 23; BD Biosciences), goat anti-KIF17 (M-20; Santa Cruz Biotechnology), and secondary antibodies conjugated to infrared dyes. Membranes were scanned with the Odyssey system.

Fluorescence microscopy and image analysis

Rat hippocampal neurons were incubated in fixation buffer (phosphate-buffered saline [PBS], 4% paraformaldehyde [PFA], 4% sucrose) for 10 min and blocked and permeabilized for 20 min with GDB (30 mM sodium phosphate, pH 7.4, 0.2% gelatin, 450 mM NaCl) and 0.05% Triton X-100. Cells were stained with the goat anti-KIF17 (1:100; M-20; Santa Cruz Biotechnology), rabbit anti-SEPT9 (1:200; Proteintech) for 4 h at room temperature and secondary donkey Alexa 594 F(ab')2 anti-goat IgG and donkey Alexa 647 F(ab')2 anti-rabbit IgG (1:200; Jackson Immunolabs, West Grove, PA) for 1 h at room temperature. Additional stainings with mouse antibodies against PSD95 (1:1000; NeuroMAb; Antibodies Incorporated, Davis, CA) and Mint1/mLin-10 (1:200; BD Biosciences, San Jose, CA) were performed with donkey Alexa 488 F(ab')2 anti-mouse IgG. In the staining controls of Supplemental Figure S2, SEPT9 and KIF17 antibodies were incubated with His-SEPT9(284-586) and KIF17 peptide (M20-P; Santa Cruz Biotechnology), respectively, for 30 min before staining. In Figure 5, A and B, GFP- and SEPT9-GFP–expressing neurons were stained for endogenous NR2B by fixing (10 min) with PBS

FIGURE 4: SEPT9 interferes with the binding of mLIn-10/Mint1 to the C-terminal tail of KIF17. (A) Coomassie-stained gels show His-SEPT9 pull down with GST-tagged KIF17(850-1029), KIF17(850-980), or KIF17(981-1029). (B) Coomassie-stained gel shows decreased binding of SEPT9 to the mutant KIF17(981-1029)EPLAAA compared with the wild-type KIF17(981-1029). (C) Coomassie-stained gel shows that mLin-10/Mint1(653-839) binding to KIF17(981-1029) decreases in the presence of SEPT9. (D) Bar graph shows relative binding of mLin-10/Mint1(653-839) to KIF17(981-1029); in the absence of SEPT9, binding was set to 1. Error bars correspond to the highest and lowest values from three independent experiments. (E) Bar graph shows the relative amount of KIF17 that coimmunoprecipitates with myc-SEPT9. Error bars correspond to the highest and lowest values from three independent experiments. (F) Western blots show that coimmunoprecipitation of GFP-mLin10 with KIF17 decreases in N2a cells that express myc-SEPT9. Input is 1% of total lysate. (G) Box-and-whisker plot shows the percentage of mLin-10/Mint-1 clusters that colocalized with KIF17, per 10 µm of dendrite in neurons expressing GFP (n = 28) or SEPT9-GFP (n = 35). Hippocampal neurons (DIV10) transfected with GFP (H) or SEPT9-GFP (I) and stained for mLin-10/Mint1 (red) and KIF17 (green). (a, b) High-magnification images show the localization of mLin-10/Mint-1 clusters with respect to KIF17 from dendrite regions outlined with dotted rectangles. Arrowheads point to colocalizing KIF17 and mLin-10 puncta. (J, K) Superresolution SIM imaging of endogenous SEPT9, KIF17, and mLin-10. Arrowheads point to KIF17/SEPT9-positive puncta that lack mLin-10 (J) and KIF17/mLin-10-positive puncta that lack SEPT9 (K).
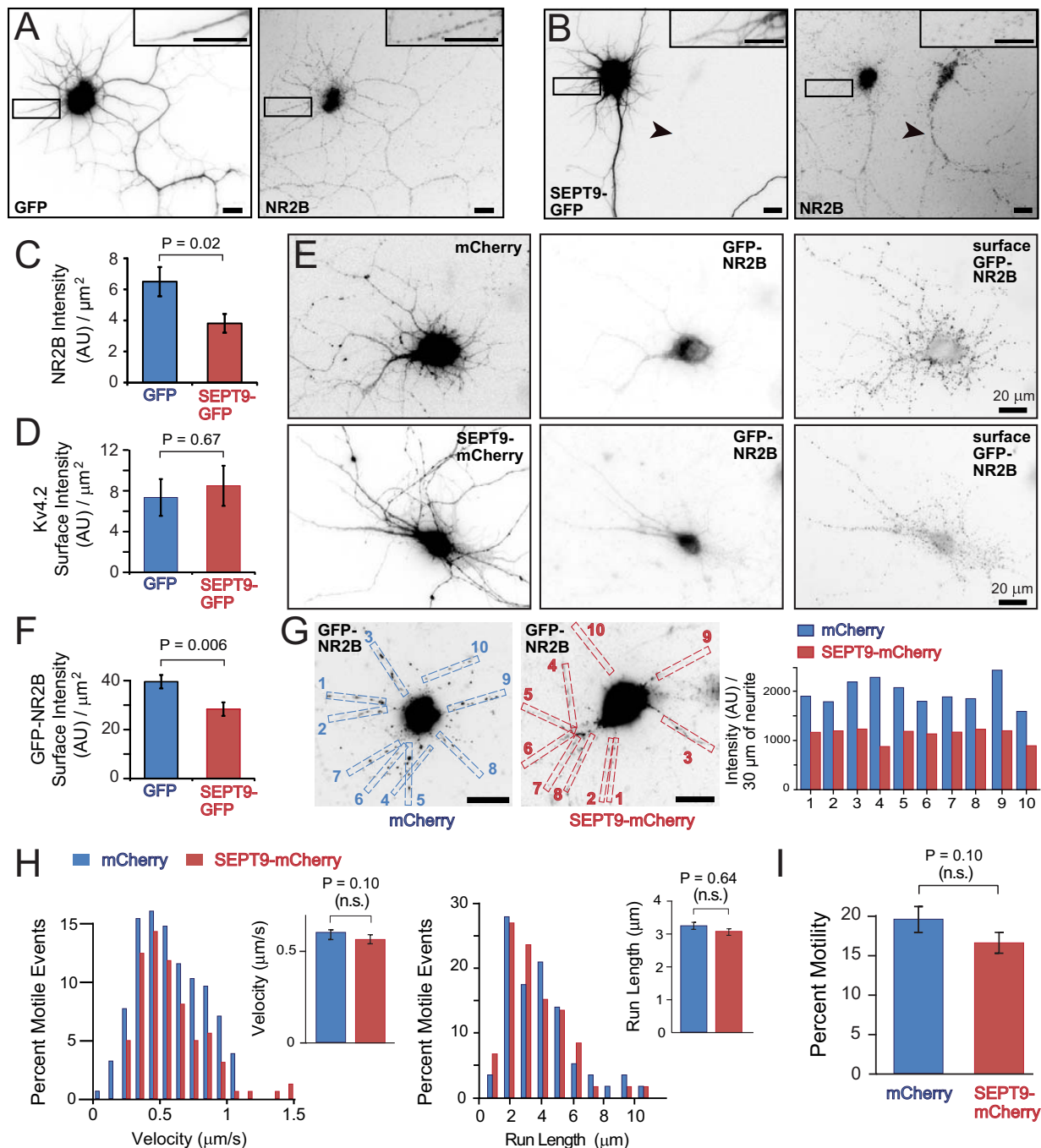
FIGURE 5: SEPT9 down-regulates NR2B transport without affecting KIF17 motility. Rat hippocampal neurons (DIV10) transfected with GFP (A) or SEPT9-GFP (B) and stained for endogenous NR2B using gentle permeabilization and fixation conditions. Insets show selected dendrite regions in high magnification (scale bars, 10 μm). Arrowhead points to an untransfected neuron. (C) Bar graph shows the mean (± SEM) fluorescence intensity of endogenous NR2B per micrometer squared for the total area of neuronal processes (18 cells). (D) Hippocampal neurons were stained live with an antibody against Kv4.2. Bar graph shows the mean (± SEM) fluorescence intensity of surface Kv4.2 per micrometer squared (20 cells). (E) Hippocampal neurons (DIV12) cotransfected with GFP-NR2B and mCherry or SEPT9-mCherry and stained live with anti-GFP to label surface GFP-NR2B. Note that mCherry and GFP channels were equally adjusted, so dendritic processes are more visible. Surface GFP-NR2B images correspond to the raw unadjusted data, which were acquired with the same exposure. (F) Bar graph shows the mean (± SEM) intensity of surface GFP-NR2B per micrometer squared for total neurite surface area (25 cells). (G) Total GFP-NR2B fluorescence in cells that express mCherry or SEPT9-mCherry (not shown). Histogram shows the sum fluorescence intensity of GFP-NR2B in the 30-μm-long regions of neurites, which are individually numbered and outlined with dotted rectangles. (H) Histograms show the distribution of the velocities ($n = 158$) and total run lengths ($n = 58$) of GFP-KIF17 in live hippocampal neurons (DIV12, $n = 8$) that express mCherry and SEPT9-mCherry. Bar graphs show the mean (± SEM) velocity and run lengths. (I) Bar graph shows the mean (± SEM) percentage of GFP-KIF17 particles that were motile in eight different neurons that express mCherry (646 particles) and SEPT9-mCherry (576 particles).

containing 4% PFA and 4% sucrose. Cells were washed with PBS and then blocked and permeabilized with GDB buffer containing 0.05% Triton X-100 for 40 min. Subsequently cells were stained with mouse antibody to NR2B (1:200; NeuroMab) and secondary donkey Alexa 594–conjugated F(ab)2 to mouse IgG (Jackson Immunolabs) in GDB buffer. In Figure 5E, neurons that were cotransfected with GFP-NR2B and mCherry or SEPT9-mCherry were stained live with rabbit anti-GFP (5 μg/ml; Invitrogen) for 10 min at 37°C. After being rinsed with cold medium, cells were incubated with fixation buffer and stained with donkey Alexa 649–conjugated secondary antibody, which was diluted in GDB buffer. In Figure 5D, the same protocol was used for the staining of endogenous surface Kv4.2 with an antibody from NeuroMab (75-016; Antibodies Incorporated). Samples were mounted in FluorSave hard mounting medium (EMD Millipore) and imaged on a Zeiss AxioObserver Z1 with a Plan Apo 63×/1.4 numerical aperture (NA) oil objective, a Hamamatsu Orca-R2 charge-coupled device camera, and SlideBook 6.0 software. Alternatively, samples were imaged with the SIM and TIRF modules of the OMX V4 microscope (GE Healthcare, Pittsburgh, PA). Superresolution SIM imaging was performed with a 60×/1.42 NA objective. A z-step size of 0.125 μm was used, and images were acquired with sCMOS pco. edge cameras (PCO) and reconstructed with softWoRx software (Applied Precision, Pittsburgh, PA).

Fluorescence quantifications per surface area of neuronal cell and neurite length were performed using a custom semiautomated MAT-LAB script that generated masks for neuronal cell bodies and processes by thresholding GFP, mCherry, SEPT9-GFP, or SEPT9-mCherry intensities. Fluorescence intensities per surface area unit were automatically calculated for each mask. Line scans of fluorescence (Figure 1D) were performed with SlideBook 6.0 software. Analysis of SEPT9, mLin-10, or PSD95 presence in KIF17 and measurements of NR2B-GFP clusters per 10 μM of dendrite were done by manual inspections of randomized dendrite regions and samples.

Live-cell imaging of hippocampal neurons was performed after cotransfection with GFP-KIF17 or GFP-KIF17(G754E) and mCherry or SEPT9-mCherry. After 48 h, coverslips were mounted on a 35-mm dish with a 7-mm-diameter bottomless hole using vacuum grease silicone. Phenol red–free Neurobasal medium supplemented with B27 (Invitrogen) and 10 mM HEPES was added, and dishes were covered and sealed with Parafilm. Samples were imaged at 37°C with TIRF microscopy on a DeltaVision OMX V4 inverted microscope (GE Healthcare) equipped with an Olympus 60×/1.49 NA objective and a temperature-controlled stage-top incubator. Images were acquired with softWoRx software, and movies were imported into Fiji software, which was used for kymograph and particle tracking analysis for the quantification of instantaneous velocities, run lengths, and percentage motility (Figure 5, H and I).

Statistical analysis

Data sets were plotted in box-and-whisker diagrams or bar graphs with R software. The whisker ends of each plot correspond to minimum and maximum values, and the top and bottom lines of each box represent the 25th (Q1) and 75th (Q3) percentiles of the data range, respectively. The median value is designated with a bold horizontal line. Statistical outliers were defined as values that were 1.5 times more than Q3 and less than Q1 values and are shown outside the whiskers of each plot. Bar graphs show mean values ± SEM (error bars). Each data set was tested for normal distribution using the Kolmogorov–Smirnov test. Mean, SEM, and p values were derived using Student's t test for normally distributed data and the Mann–Whitney U test for nonnormal data in GraphPad Prism software.

REFERENCES
Acharya BR, Espenel C, Kreitzer G (2013). Direct regulation of microtubule dynamics by KIF17 motor and tail domains. J Biol Chem 288, 32302–32313.

Akhmanova A, Hammer JA 3rd (2010). Linking molecular motors to membrane cargo. Curr Opin Cell Biol 22, 479–487.

Atherton J, Houdusse A, Moores C (2013). MAPping out distribution routes for kinesin couriers. Biol Cell 105, 465–487.

Bai X, Bowen JR, Knox TK, Zhou K, Pendziwiat M, Kuhlenbaumer G, Sindelar CV, Spiliotis ET (2013). Novel septin 9 repeat motifs altered in neuralgic amyotrophy bind and bundle microtubules. J Cell Biol 203, 895–905.

Barria A, Malinow R (2002). Subunit-specific NMDA receptor trafficking to synapses. Neuron 35, 345–353.

Baust T, Anitei M, Czupalla C, Parshyna I, Bourel L, Thiele C, Krause E, Hoflack B (2008). Protein networks supporting AP-3 function in targeting lysosomal membrane proteins. Mol Biol Cell 19, 1942–1951.

Bielska E, Schuster M, Roger Y, Berepiki A, Soanes DM, Talbot NJ, Steinberg G (2014). Hook is an adapter that coordinates kinesin-3 and dynein cargo attachment on early endosomes. J Cell Biol 204, 989–1007.

Blasius TL, Cai D, Jih GT, Toret CP, Verhey KJ (2007). Two binding partners cooperate to activate the molecular motor Kinesin-1. J Cell Biol 176, 11–17.

Caudron F, Barral Y (2009). Septins and the lateral compartmentalization of eukaryotic membranes. Dev Cell 16, 493–506.

Chu PJ, Rivera JF, Arnold DB (2006). A role for Kif17 in transport of Kv4.2. J Biol Chem 281, 365–373.

Dishinger JF, Kee HL, Jenkins PM, Fan S, Hurd TW, Hammond JW, Truong YN, Margolis B, Martens JR, Verhey KJ (2010). Ciliary entry of the kinesin-2 motor KIF17 is regulated by importin-beta2 and RanGTP. Nat Cell Biol 12, 703–710.

Dolat L, Hunyara JL, Bowen JR, Karasmanis EP, Elgawly M, Galkin VE, Spiliotis ET (2014). Septins promote stress fiber-mediated maturation of focal adhesions and renal epithelial motility. J Cell Biol 207, 225–235.

Espenel C, Acharya BR, Kreitzer G (2013). A biosensor of local kinesin activity reveals roles of PKC and EB1 in KIF17 activation. J Cell Biol 203, 445–455.

Fu MM, Holzbaur EL (2013). JIP1 regulates the directionality of APP axonal transport by coordinating kinesin and dynein motors. J Cell Biol 202, 495–508.

Fu MM, Holzbaur EL (2014). Integrated regulation of motor-driven organelle transport by scaffolding proteins. Trends Cell Biol 24, 564–574.

Gonzalez ME, Makarova O, Peterson EA, Privette LM, Petty EM (2009). Up-regulation of SEPT9_v1 stabilizes c-Jun-N-terminal kinase and contributes to its pro-proliferative activity in mammary epithelial cells. Cell Signal 21, 477–487.

Guillaud L, Setou M, Hirokawa N (2003). KIF17 dynamics and regulation of NR2B trafficking in hippocampal neurons. J Neurosci 23, 131–140.

Hammond JW, Blasius TL, Soppina V, Cai D, Verhey KJ (2010). Autoinhibition of the kinesin-2 motor KIF17 via dual intramolecular mechanisms. J Cell Biol 189, 1013–1025.

Hirokawa N, Noda Y, Tanaka Y, Niwa S (2009). Kinesin superfamily motor proteins and intracellular transport. Nat Rev Mol Cell Biol 10, 682–696.

Hu J, Bai X, Bowen JR, Dolat L, Korobova F, Yu W, Baas PW, Svitkina T, Gallo G, Spiliotis ET (2012). Septin-driven coordination of actin and microtubule remodeling regulates the collateral branching of axons. Curr Biol 22, 1109–1115.

Hu Q, Milenkovic L, Jin H, Scott MP, Nachury MV, Spiliotis ET, Nelson WJ (2010). A septin diffusion barrier at the base of the primary cilium maintains ciliary membrane protein distribution. Science 329, 436–439.

Jaulin F, Kreitzer G (2010). KIF17 stabilizes microtubules and contributes to epithelial morphogenesis by acting at MT plus ends with EB1 and APC. J Cell Biol 190, 443–460.

Jenkins PM, Hurd TW, Zhang L, McEwen DP, Brown RL, Margolis B, Verhey KJ, Martens JR (2006). Ciliary targeting of olfactory CNG channels requires the CNGB1b subunit and the kinesin-2 motor protein, KIF17. Curr Biol 16, 1211–1216.

Jo K, Derin R, Li M, Bredt DS (1999). Characterization of MALS/Velis-1, -2, and -3: a family of mammalian LIN-7 homologs enriched at brain synapses in association with the postsynaptic density-95/NMDA receptor postsynaptic complex. J Neurosci 19, 4189–4199.

Kayadjanian N, Lee HS, Pina-Crespo J, Heinemann SF (2007). Localization of glutamate receptors to distal dendrites depends on subunit composition and the kinesin motor protein KIF17. Mol Cell Neurosci 34, 219–230.

Kim MS, Froese CD, Estey MP, Trimble WS (2011). SEPT9 occupies the terminal positions in septin octamers and mediates polymerization-dependent functions in abscission. J Cell Biol 195, 815–826.

Kinoshita M (2006). Diversity of septin scaffolds. Curr Opin Cell Biol 18, 54–60.

Kinoshita N, Kimura K, Matsumoto N, Watanabe M, Fukaya M, Ide C (2004). Mammalian septin Sept2 modulates the activity of GLAST, a glutamate transporter in astrocytes. Genes Cells 9, 1–14.

Macho B, Brancorsini S, Fimia GM, Setou M, Hirokawa N, Sassone-Corsi P (2002). CREM-dependent transcription in male germ cells controlled by a kinesin. Science 298, 2388–2390.

Matos MF, Xu Y, Dulubova I, Otwinowski Z, Richardson JM, Tomchick DR, Rizo J, Ho A (2012). Autoinhibition of Mint1 adaptor protein regulates amyloid precursor protein binding and processing. Proc Natl Acad Sci USA 109, 3802–3807.

Mostowy S, Cossart P (2012). Septins: the fourth component of the cytoskeleton. Nat Rev Mol Cell Biol 13, 183–194.

Nagata K, Kawajiri A, Matsui S, Takagishi M, Shiromizu T, Saitoh N, Izawa I, Kiyono T, Itoh TJ, Hotani H, Inagaki M (2003). Filament formation of MSF-A, a mammalian septin, in human mammary epithelial cells depends on interactions with microtubules. J Biol Chem 278, 18538–18543.

Sellin ME, Sandblad L, Stenmark S, Gullberg M (2011). Deciphering the rules governing assembly order of mammalian septin complexes. Mol Biol Cell 22, 3152–3164.

Sellin ME, Stenmark S, Gullberg M (2012). Mammalian SEPT9 isoforms direct microtubule-dependent arrangements of septin core heteromers. Mol Biol Cell 23, 4242–4255.

Setou M, Nakagawa T, Seog DH, Hirokawa N (2000). Kinesin superfamily motor protein KIF17 and mLin-10 in NMDA receptor-containing vesicle transport. Science 288, 1796–1802.

Sirajuddin M, Rice LM, Vale RD (2014). Regulation of microtubule motors by tubulin isotypes and post-translational modifications. Nat Cell Biol 16, 335–344.

Spiliotis ET, Gladfelter AS (2012). Spatial guidance of cell asymmetry: septin GTPases show the way. Traffic 13, 195–203.

Spiliotis ET, Hunt SJ, Hu Q, Kinoshita M, Nelson WJ (2008). Epithelial polarity requires septin coupling of vesicle transport to polyglutamylated microtubules. J Cell Biol 180, 295–303.

Spiliotis ET, Kinoshita M, Nelson WJ (2005). A mitotic septin scaffold required for Mammalian chromosome congression and segregation. Science 307, 1781–1785.

Sun F, Zhu C, Dixit R, Cavalli V (2011). Sunday Driver/JIP3 binds kinesin heavy chain directly and enhances its motility. EMBO J 30, 3416–3429.

Tada T, Simonetta A, Batterton M, Kinoshita M, Edbauer D, Sheng M (2007). Role of Septin cytoskeleton in spine morphogenesis and dendrite development in neurons. Curr Biol 17, 1752–1758.

Takano K, Miki T, Katahira J, Yoneda Y (2007). NXF2 is involved in cytoplasmic mRNA dynamics through interactions with motor proteins. Nucleic Acids Res 35, 2513–2521.

Tsang CW, Estey MP, DiCiccio JE, Xie H, Patterson D, Trimble WS (2011). Characterization of presynaptic septin complexes in mammalian hippocampal neurons. Biol Chem 392, 739–749.

Verhey KJ, Gaertig J (2007). The tubulin code. Cell Cycle 6, 2152–2160.

Verhey KJ, Hammond JW (2009). Traffic control: regulation of kinesin motors. Nat Rev Mol Cell Biol 10, 765–777.

Verhey KJ, Meyer D, Deehan R, Blenis J, Schnapp BJ, Rapoport TA, Margolis B (2001). Cargo of kinesin identified as JIP scaffolding proteins and associated signaling molecules. J Cell Biol 152, 959–970.

Walenta JH, Didier AJ, Liu X, Kramer H (2001). The Golgi-associated hook3 protein is a member of a novel family of microtubule-binding proteins. J Cell Biol 152, 923–934.

Wong-Riley MT, Besharse JC (2012). The kinesin superfamily protein KIF17: one protein with many functions. Biomol Concepts 3, 267–282.

Xie Y, Vessey JP, Konecna A, Dahm R, Macchi P, Kiebler MA (2007). The GTP-binding protein Septin 7 is critical for dendrite branching and dendritic-spine morphology. Curr Biol 17, 1746–1751.

Yin X, Feng X, Takei Y, Hirokawa N (2012). Regulation of NMDA receptor transport: a KIF17-cargo binding/releasing underlies synaptic plasticity and memory in vivo. J Neurosci 32, 5486–5499.

Yin X, Takei Y, Kido MA, Hirokawa N (2011). Molecular motor KIF17 is fundamental for memory and learning via differential support of synaptic NR2A/2B levels. Neuron 70, 310–325.

Zhu M, Wang F, Yan F, Yao PY, Du J, Gao X, Wang X, Wu Q, Ward T, Li J, et al. (2008). Septin 7 interacts with centromere-associated protein E and is required for its kinetochore localization. J Biol Chem 283, 18916–18925.